Human Molecular Genetics, 2019, Vol. 28, No. 20 3475–3485

doi: 10.1093/hmg/ddz159
Advance Access Publication Date: 13 September 2019
General Article

GENERAL ARTICLE

Hypoxic drive caused type 3 neovascularization in a preclinical model of exudative age-related macular degeneration

Lijuan Zhang[1,*,†], Xuan Cui[2,3,4,†], Yangjun Han[5], Karen Sophia Park[3,4], Xiaohong Gao[1], Ximei Zhang[1], Zhigang Yuan[1], Yong Hu[6], Chun-Wei Hsu[3,4], Xiaorong Li[2], Alexander G. Bassuk[7], Vinit B. Mahajan[8,9], Nan-Kai Wang[3,4] and Stephen H. Tsang[3,4,10,*]

[1]Shanxi Eye Hospital, affiliated with Shanxi Medical University. Fudong St. 100, Xinghualing, Taiyuan, Shanxi 030002, China [2]Tianjin Medical University Eye Hospital, Tianjin Medical University Eye Institute & Tianjin Medical University School of Optometry and Ophthalmology, Tianjin 300384, China, New York, NY10032, USA [3]Jonas Children's Vision Care and the Bernard & Shirlee Brown Glaucoma Laboratory, Herbert Irving Comprehensive Cancer Center, New York, NY 10032, USA [4]Edward S. Harkness Eye Institute, New York-Presbyterian Hospital, New York, NY 10032, USA [5]Shanxi Cardiovascular Disease Hospital, Yifen street 18, Wanbailin, Taiyuan, Shanxi 030024, China [6]Department of Neurology, Shanghai Tongji Hospital, Tongji University School of Medicine, Shanghai 200092, China [7]Department of Pediatrics, University of Iowa, Iowa City, IA 52242, USA [8]Byers Eye Institute, Omics Laboratory, Department of Ophthalmology, Stanford University School of Medicine, Palo Alto, CA 94303, USA [9]Veterans Affairs Palo Alto Health Care System, Palo Alto, CA 94304, USA and [10]Department of Pathology & Cell Biology, Stem Cell Initiative (CSCI), Institute of Human Nutrition, College of Physicians and Surgeons, Columbia University, New York, NY 10032, USA

*To whom correspondence should be addressed at: Stephen H. Tsang, M.D., PhD, Edward S. Harkness Eye Institute, New York-Presbyterian Hospital/Columbia University Medical Center, 635 West 165th Street, Box 112, New York, NY 10032, USA. Tel: 212-342-1186; Fax: 212-305-4987; Email: sht2@columbia.edu. Lijuan Zhang, MD, PhD, Shanxi Eye Hospital, affiliated with Shanxi Medical University, 100 Fudong St., Xinghualing, Taiyuan, Shanxi 030002, China. Email: Zhanglj2004@163.com

Abstract

Hypoxia associated with the high metabolic demand of rods has been implicated in the pathology of age-related macular degeneration (AMD), the most common cause of adult blindness in the developed world. The majority of AMD-associated severe vision loss cases are due to exudative AMD, characterized by neovascularization. To further investigate the causes and histopathology of exudative AMD, we conditionally induced hypoxia in a novel preclinical AMD model ($Pde6g^{creERT2/+};Vhl^{-/-}$) by targeting *Vhl* and used multimodal imaging and immunohistochemistry to track the development of hypoxia-induced neovascularization. In addition to developing a preclinical model that phenocopies exudative AMD, our studies revealed that the photoreceptor hypoxic response initiates and drives type 3 neovascularization, mainly in the outer retina. Activation of the VHL-HIF1a-VEGF-EPO pathway in the adult retina led to long-term neovascularization, retinal

[†]The authors wish it to be known that, in their opinion, the first two authors should be regarded as joint First Authors.

Received: March 29, 2019. **Revised:** March 29, 2019. **Accepted:** July 1, 2019

hemorrhages and compromised retinal layers. Our novel preclinical model would accelerate the testing of therapies that use metabolomic approaches to ameliorate AMD.

Introduction

Rod photoreceptors are the most numerous and metabolically demanding cells in the retina (1–4). Hypoxia associated with the high energy demand of rod photoreceptors has been implicated in diabetic retinopathy and age-related macular degeneration (AMD), a significant public health concern worldwide (5–7). AMD is characterized by irreversible damage to the central region of the retina, disabling patients from participating in activities of daily living including recognizing faces, reading and driving (8). Exudative or 'wet' AMD, primarily characterized by substantial neovascularization and subsequent capillary leakage, is less common than dry AMD but accounts for approximately 80–90% of all cases of severe vision loss (5,9–11). Three types of exudative AMD were described based on the location of neovascularization in the retina: type 1 ['occult', 'sub-RPE', under the retinal pigment epithelium (RPE) layer], type 2 ('classic', 'subretinal', under the photoreceptor layer) and type 3 ('intraretinal', choroidal anastomisis spanning the retina and choroid) neovascularization.

The significant role of rods in AMD pathogenesis is reflected in the widespread use of panretinal photocoagulation (PRP); PRP has reduced the incidence of AMD by ablating the high energy-demanding photoreceptors in the outer retina and decreasing the number of rods, thereby lowering the burden of oxygen demand and hypoxia (3,12). Studies have shown that years of chronic photoreceptor hypoxia caused by the thickening of Bruch's membrane, accumulation of drusen and consequent reduction of choroidal blood flow—the primary oxygen source of photoreceptors—can initiate AMD (13).

Important pathological mechanisms of angiogenesis in AMD involve hypoxia-induced factors (HIFs), which transcribe proteins typically generated in low-oxygen cellular environments. Hypoxic conditions can be recapitulated in animal models by activating HIFs such as HIF1a, which acts as a key transcription factor during hypoxic conditions by mediating the upregulation of VEGF (14). Although pharmaceuticals targeting VEGF have been successfully applied to suppress neovascularization in exudative AMD, limited data are available on the underlying mechanism of how the treatment acts to restore hypoxia (15). In addition, it remains unclear as to how hypoxic conditions precisely lead to neovascularization in specific retinal layers (16).

Under normoxic conditions, the von Hippel Lindau (VHL) protein is an E3 ubiquitin ligase that inhibits HIF activity through the detection and ubiquitinization of hydroxylated HIF alpha subunits (17). Thus, the *Vhl* gene is a target for the inactivation of HIF and subsequent upregulation of hypoxia-induced proteins (18). In this study, we used a *Pde6g* $^{creERT2/+}$ driver to ablate *Vhl*, allowing us to investigate the origin and consequences of hypoxia-induced pathology.

Results

Intact retinal vasculature in the *Pde6g*$^{creERT2/+}$;*Vhl*$^{flox/flox}$ control mouse model on multimodal fundus imaging

Multimodal imaging centered on or to the right of the optic nerve was obtained from 6-week-old *Pde6g*$^{creERT2/+}$;*Vhl*$^{flox/flox}$ control mice (Fig. 1). Infrared (IR) fundus images showed vessels in dark grey with no detectable abnormalities (Fig. 1A and C). Fundus fluorescein angiography (FFA) images from *Pde6g*$^{creERT2/+}$; *Vhl*$^{+/+}$ mice showed normal retinal vasculature with no neovascularization or leakage (Fig. 1B and D). A horizontal optical coherence tomography (OCT) scan of the fundus of *Pde6g*$^{creERT2/+}$;*Vhl*$^{flox/flox}$ control mice suggested preserved retinal structure with normal retinal thickness and clearly defined layers (Fig. 1E).

Induced hypoxia caused retinal neovascularization in both neonatal and mature *Pde6g*$^{creERT2/+}$;*Vhl* $^{-/-}$ mice

Tamoxifen was administered to *Pde6g*$^{creERT2/+}$; *Vhl* $^{flox/flox}$ mice for three consecutive days starting from P7 in order to observe the effects of *Vhl* knockout in the neonatal retina. IR and FFA images were acquired at 4, 6, 8 and 16 weeks post-tamoxifen injection. AK-Fluor was intraperitoneally injected into the mice as described in the Materials and Methods. IR images at 4 weeks showed equably grey color in the fundus, with one circular lesion depicted in lighter grey in the middle of the fundus (Fig. 2A). FFA images showed normal vessels without leakage at the early phase (Fig. 2B), while leakage appeared at the middle phase (Fig. 2C) and intensified at the late phase (Fig. 2D). The areas of leakage coincided with the light grey lesions found in the IR images. A single white lesion was found in 12 out of 20 total eyes at 4 weeks in *Pde6g*$^{creERT2/+}$;*Vhl* $^{-/-}$ mice, while more light grey lesions on the fundus were found at 6 weeks in the IR images (Fig. 2E). Leakage was sparsely detected in the early phase, while it was easier to recognize at middle and late phases at 6 weeks (Fig. 2F–H). With the optic nerve oriented at the center of the fundus image, there were 3–10 lesion areas dispersed across the fundus when viewed through the 55° lens at week 6 in all 22 eyes. More light grey lesions were found at 8 and 16 weeks (Fig. 2I and M) with leakage starting from the early phase (Fig. 2J–P); specifically, 6–14 lesion areas were found in all 24 eyes at week 8 while 7–16 lesion areas were found in all 12 eyes at week 16. The size of the lesions was observed to be greater at 16 weeks than at 8 weeks due to the fusion of multiple smaller lesions.

To observe the effects of induced hypoxia in the mature retina, tamoxifen was also administered to *Pde6g*$^{creERT2/}$;*Vhl* $^{flox/flox}$ mice for 3 consecutive days starting from P28, at which time the mice were considered mature. IR and FFA images were taken at 6, 8, 10 and 16 weeks. In contrast to the neonatal mice with tamoxifen injected at P7, the mature mice exhibited normal vessels and a healthy phenotype at 6 weeks (Fig. 3A–D). While the IR images showed no abnormalities in all eight eyes at week 8 (Fig. 3E), several white dots on FFA were observed throughout the fundus in four eyes (Fig. 3F–H), and a single lesion was found in the fundus of two eyes, similar to the phenotype shown in Figure 2D. Lesions depicted in light grey were found in IR images at week 10 (Fig. 3I), with leakages visible from the early phase at this time point (Fig. 3J–L). Even more lesions and severe leakages were observed at 16 weeks (Fig. 3M–P). On the 55° lens, 3–6 lesions were found in the fundus of 7 out of 8 eyes while a single lesion was found in 1 eye at 10 weeks. About 4–10 lesions of varying sizes were detected in all 8 eyes at 16 weeks.

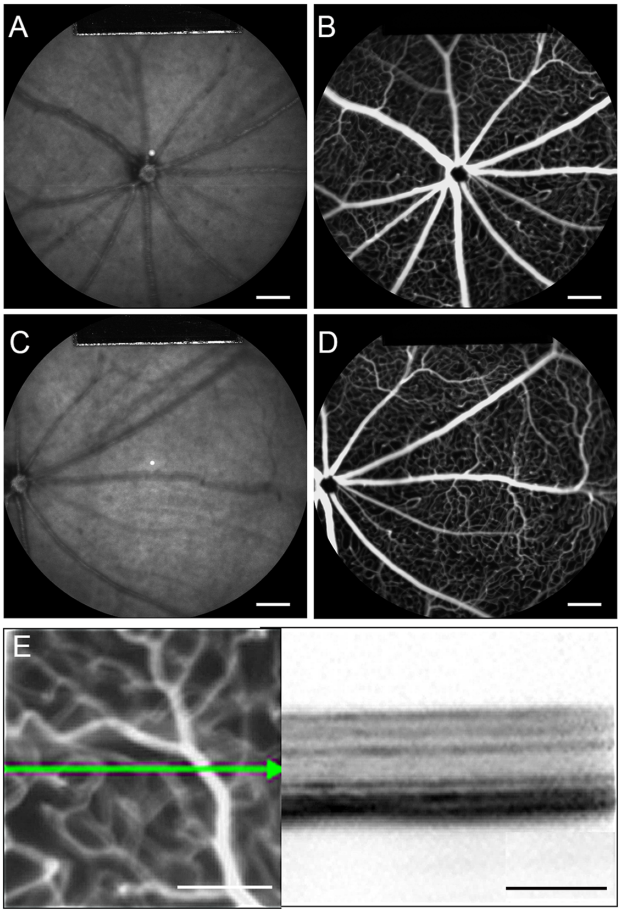

Figure 1. Multimodal live images of retina from *Pde6g*$^{creERT2/+}$;*Vhl*$^{flox/flox}$ control mouse displays intact retinal vasculature. (**A** and **C**) Fundus IR imaging (800 nm) of the *Pde6g*$^{creERT2/+}$;*Vhl* $^{flox/flox}$ mouse model centered on the optic disc. (**B** and **D**) FFA of the fundus using fluorescein dye and a blue (488 nm) laser stimulus. (**E**) OCT cross section of *Pde6g*$^{creERT2/+}$;*Vhl* $^{flox/flox}$ using near-IR reflectance (820 nm) modalities. A and B are centered on the optic disc. C and D were used to observe the peripheral retina with the optic disc centered on the left. (white scale bar = 1 mm; black scale bar = 200 µm; green arrow = OCT scan)

In sum, comparable levels of neovascularization were seen after tamoxifen administration at either P7 or P28. As such, given that both neonatal and mature retinae responded to hypoxia induction, our findings suggest that photoreceptor hypoxia is sufficient to cause neovascularization regardless of the developmental stage of the deep vascular bed.

Abnormal structures related to neovascularization in the deep retina were found on OCT imaging

OCT cross sections were imaged over the leakage sites shown in the FFA images to observe the effects of *Vhl* knockout on the integrity of the retinal layers. Compared to the well-preserved retinal layers of the control *Pde6g*$^{creERT2/+}$;*Vhl*$^{flox/flox}$ mouse model on OCT (Fig. 4A), the individual layers of the mutant *Pde6g*$^{creERT2/+}$;*Vhl*$^{-/-}$ model appear more blurred and indistinguishable. An RPE tear (Fig. 4B), lifted IS/OS layer (Fig. 4C), non-intact Bruch's membrane associated with an abnormal structure in the choroid (Fig. 4D), subretinal fluid (Fig. 4E) and hyperreflectivity in the outer retina (Fig. 4F) were found in the *Pde6g*$^{creERT2/+}$;*Vhl*$^{-/-}$ mouse model.

Activation of the VHL-HIF1a-VEGF-EPO signaling in *Pde6g*$^{creERT2/+}$;*Vhl*$^{-/-}$ mouse retina

Tamoxifen was applied for three consecutive days from P7 to *Pde6g*$^{creERT2/+}$;*Vhl*$^{flox/flox}$ mice in order to ablate *Vhl* specifically in rod photoreceptor cells, while sham injection was applied as a control to *Pde6g*$^{creERT2/+}$; *Vhl*$^{flox/flox}$ mice at the same age. Retinae from both groups were harvested at 4 weeks post-injection. VHL could be detected in the outer nuclear layer (ONL) of the *Pde6g*$^{creERT2/+}$;*Vhl*$^{flox/flox}$ mice, while no VHL signal was seen in that of the *Pde6g*$^{creERT2/+}$;*Vhl*$^{-/-}$ mouse retina (Fig. 5A). VEGF expressed mostly in the inner plexiform layer (IPL) in the *Pde6g*$^{creERT2/+}$;*Vhl*$^{flox/flox}$ mice, while a stronger signal was found in the IPL, ONL and inner nuclear layer (INL) after rod *Vhl* inactivation in the *Pde6g*$^{creERT2/+}$;*Vhl*$^{-/-}$ mice (Fig. 5B). HIF1a signals were observed mostly in the IPL and INL in *Pde6g*$^{creERT2/+}$;*Vhl*$^{flox/flox}$ mice, compared to *Pde6g*$^{creERT2/+}$;*Vhl*$^{-/-}$ mice that demonstrated presence of HIF1a in the photoreceptor layer and INL (Fig. 5C). A similar phenomenon was also observed with EPO, which was not detected in the ONL layer in *Pde6g*$^{creERT2/+}$;*Vhl*$^{flox/flox}$ mice but upregulated in the photoreceptor layer of *Pde6g*$^{creERT2/}$;*Vhl*$^{-/-}$ mice (Fig. 5D). Our immunostaining results suggest that tamoxifen-induced knockout of *Vhl* in the mouse retina activated the VHL-HIF1a-VEGF-EPO pathway, thereby successfully inducing hypoxic conditions. To ensure that retina-specific hypoxic conditions were induced, irises of *Pde6g*$^{creERT2/+}$;*Vhl*$^{-/-}$ mice were also collected at 10 weeks and subject to FFA imaging. The vessels were clearly detected without neovascularization or leakage, suggesting that hypoxic conditions were limited to the retina (Supplementary Material, Fig. S1).

Long-term significant neovascularization, exudation and retinal detachment were found in the subretinal space after induced hypoxia in photoreceptor cells.

The *Pde6g*$^{creERT2/+}$;*Vhl* $^{-/-}$ mouse model was generated with tamoxifen injected for three consecutive days from P7. To assess the long-term stability of neovascularization in our *Pde6g*$^{creERT2/+}$;*Vhl* $^{-/-}$ model, optic cups were harvested and stained at 6 weeks (Fig. 6A–E), 10 weeks (Fig. 6F–J) and 16 weeks (Fig. 6K–O). An abnormal subretinal neovascularization bulb and mass (Fig. 6A and B), RPE break (Fig. 6C), RPE-wrapped lesion (Fig. 6D) and subretinal hemorrhage were discovered in the *Pde6g*$^{creERT2/+}$;*Vhl*$^{-/-}$ model at 6 weeks. All such phenotypes were found to be stable and reproducible at both 10 (Fig. 6F–J) and 16 (Fig. 6K–O) weeks.

At 10 weeks, optic cups from the control and mutant groups were harvested, and periodic acid schiff (PAS; Fig. 7A–H) and immunofluorescence (Fig. 7I–L) staining were performed. In the 10-week-old *Pde6g*$^{creERT2/+}$;*Vhl* $^{flox/flox}$ mouse model (Fig. 7A, E and I), the retinal structure was well preserved, and the vessels could only be detected in the outer plexiform layer (OPL), IPL and ganglion cell layer (GCL). In the PAS staining images of the *Pde6g*$^{creERT2/+}$;*Vhl*$^{-/-}$ mouse model, the retinal integrity was significantly compromised given the disturbed ONL, enveloped and migrated RPE and formation of subretinal hemorrhages (Fig. 7B–D and F–H). The RPE layer and Bruch's membrane appeared to be deteriorated and contaminated with blood cells. In the immunofluorescence images of anti-CD31, a vessel marker, the vessels could be detected in all of the retinal layers from the GCL to the photoreceptor layer, subretinal layer and sub-RPE layer (Fig. 7G–L). The vessels in the ONL appeared to be connected with those found in the subretinal space and sub-RPE layer.

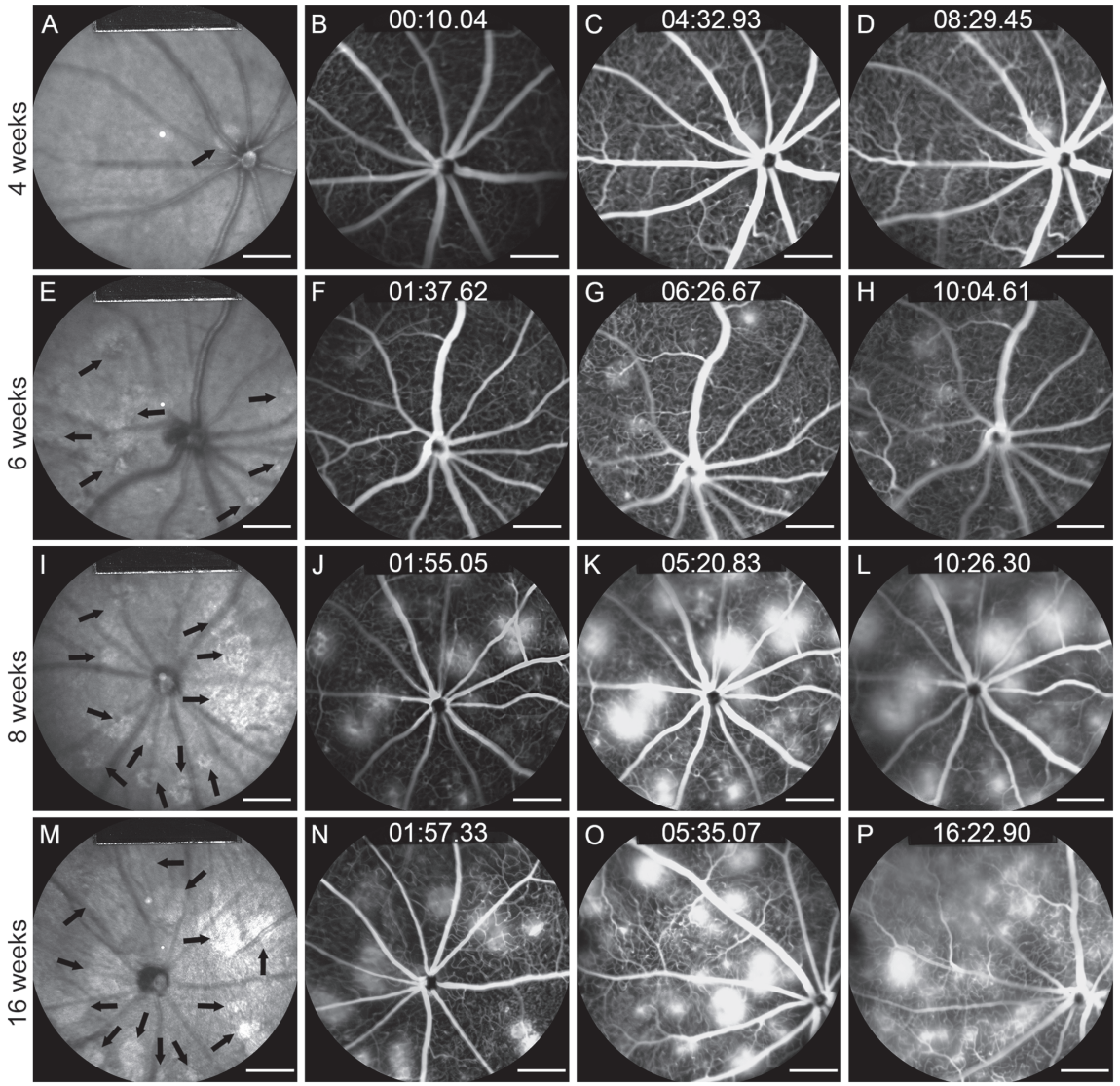

Figure 2. IR imaging and fluorescein angiography show progressive neovascularization and leakage after HIF induction at postnatal day 7. Tamoxifen was administered to the *Pde6g*$^{creERT2/+}$;*Vhl*$^{flox/flox}$ mouse model at P7 for 3 days. (**A**, **E**, **I** and **M**) IR images of the fundus were collected at 4, 6, 8 and 16 weeks. Black arrows indicate hyporeflective lesion areas. FFA images were collected at early, middle and late phases at weeks 4 (**B–D**), 6 (**F–H**), 8 (**J–L**) and 16 (**N–P**) (scale bar = 1 mm).

3D confocal imaging revealed neovascularization in the deep retinal vasculature of the 6-week *Pde6g*$^{creERT2/+}$;*Vhl*$^{-/-}$ mouse model

Tamoxifen was injected at P7 for three consecutive days in *Pde6g*$^{creERT2/+}$;*Vhl* $^{flox/flox}$ mice to generate the *Pde6g*$^{creERT2/+}$;*Vhl* $^{-/-}$ mouse model, while sham injection was applied to the *Pde6g*$^{creERT2/+}$;*Vhl* $^{flox/flox}$ mouse model as a control at the same age. Immunofluorescence staining was applied to the mouse retina of both 6-week *Pde6g*$^{creERT2/+}$;*Vhl*$^{flox/flox}$ (Fig. 8A) and *Pde6g*$^{creERT2/+}$;*Vhl* $^{-/-}$ (Fig. 8B) mouse models. 3D modeling of the retinal vasculature revealed that the retinal capillary network was thicker in the *Pde6g*$^{creERT2/+}$;*Vhl* $^{-/-}$ mouse model than in the *Pde6g*$^{creERT2/+}$;*Vhl* $^{flox/flox}$ mouse model (Fig. 8C), suggesting abnormal neovascularization. The vessels appeared more numerous throughout the retinal layers with greater curvature and branching in the mutant model as compared to the control.

Discussion

Our studies using a novel preclinical mouse model of AMD, *Pde6g*$^{creERT2/+}$;*Vhl*$^{-/-}$, validated the hypothesis that hypoxic responses in photoreceptors are both an initiator and a driver of type 3 neovascularization. Age-related thickening of Bruch's membrane is known to cause a progressive decrease in the diffusion capacity of oxygen from the choriocapillaris to the photoreceptors in humans (6,13). Vascular abnormalities typically associated with such age-related changes in advanced-stage patients with exudative AMD manifested in our *Pde6g*$^{creERT2/+}$;*Vhl*$^{-/-}$ mice as type 3 neovascularization.

The rod photoreceptor-specific *Pde6g*$^{creERT2/+}$ driver induced hypoxic responses, and the resulting *Pde6g*$^{creERT2/+}$;*Vhl*$^{-/-}$ mice successfully recapitulated photoreceptor hypoxia as evidenced by the activation of the VHL-HIF1a-VEGF-EPO pathway. Live fluorescein angiography displayed microaneurysms and leakages on the fundus, which were indicative of retinal

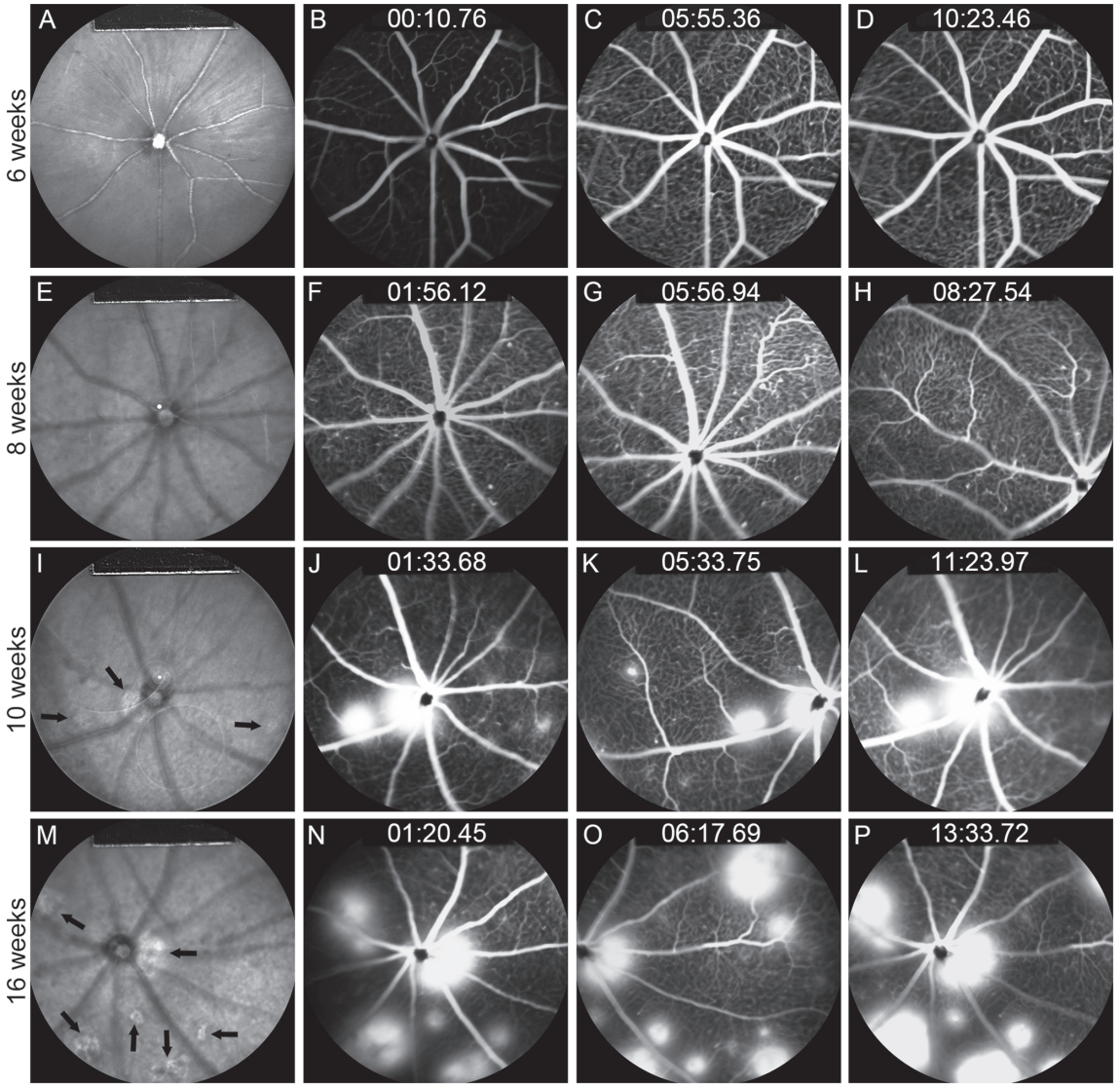

Figure 3. IR imaging and fluorescein angiography show progressive neovascularization and leakage after HIF induction at postnatal day 28. Tamoxifen was administered to the *Pde6g*$^{creERT2/+}$;*Vhl*$^{flox/flox}$ mouse model at P28 for 3 days. (**A**, **E**, **I** and **M**) IR images were taken at 6, 8, 10 and 16 weeks. Black arrows indicate *hyperreflective* lesions. FFA images were collected at early, middle and late phases at weeks 6 (**B–D**), 8 (**F–H**), 10 (**J–L**) and 16 (**N–P**).

neovascularization. Immunofluorescence staining of the retinal vessels revealed that the neovascularization was localized to the ONL, inner/outer segment layer and subretinal layer—areas in which abnormal retinal vessel growth was not observed in controls. We additionally found that both young and adult *Pde6g*$^{creERT2/+}$;*Vhl*$^{flox/flox}$ retinae responded to hypoxia induction and showed comparable levels of intraretinal and subretinal neovascularization, supporting the conclusion that hypoxia-induced neovascularization may occur independent of the age of the retinal vascular bed. Our novel results, produced by the hypoxia-driven upregulation of VEGF, validate previous studies that have observed neovascularization in the deep capillary bed in rhodopsin-VEGF transgenic mice (19).

Many previous mouse models of neovascularization have only achieved partial success in mimicking exudative AMD. In the *Vldlr* $^{-/-}$ neovascularization model, for example, although the disease phenotype consisted of choroidal anastomosis and retinal hemorrhage, the manifestation had been systemic rather than isolated to the retina (20,21). Other neovascularization models have overexpressed VEGF in the RPE through subretinal injection. In one case, subretinal injection of VEGF in mice successfully caused angiographic leakage within the localization area 1 week after injection (22). In other cases, neovascularization was robust at 4 weeks after VEGF injection and could last as long as 20 months post-injection (23–25). The drawbacks of developing these models, however, are that (1) subretinal injection may itself cause trauma to the retina, and (2) the lesion caused by the injection does cover the entire retina, limiting the accuracy of the resulting disease phenotype. Such complications and drawbacks highlight the need for a more reliable and accurate AMD animal model, which could assist significantly in developing targeted therapeutics for exudative AMD.

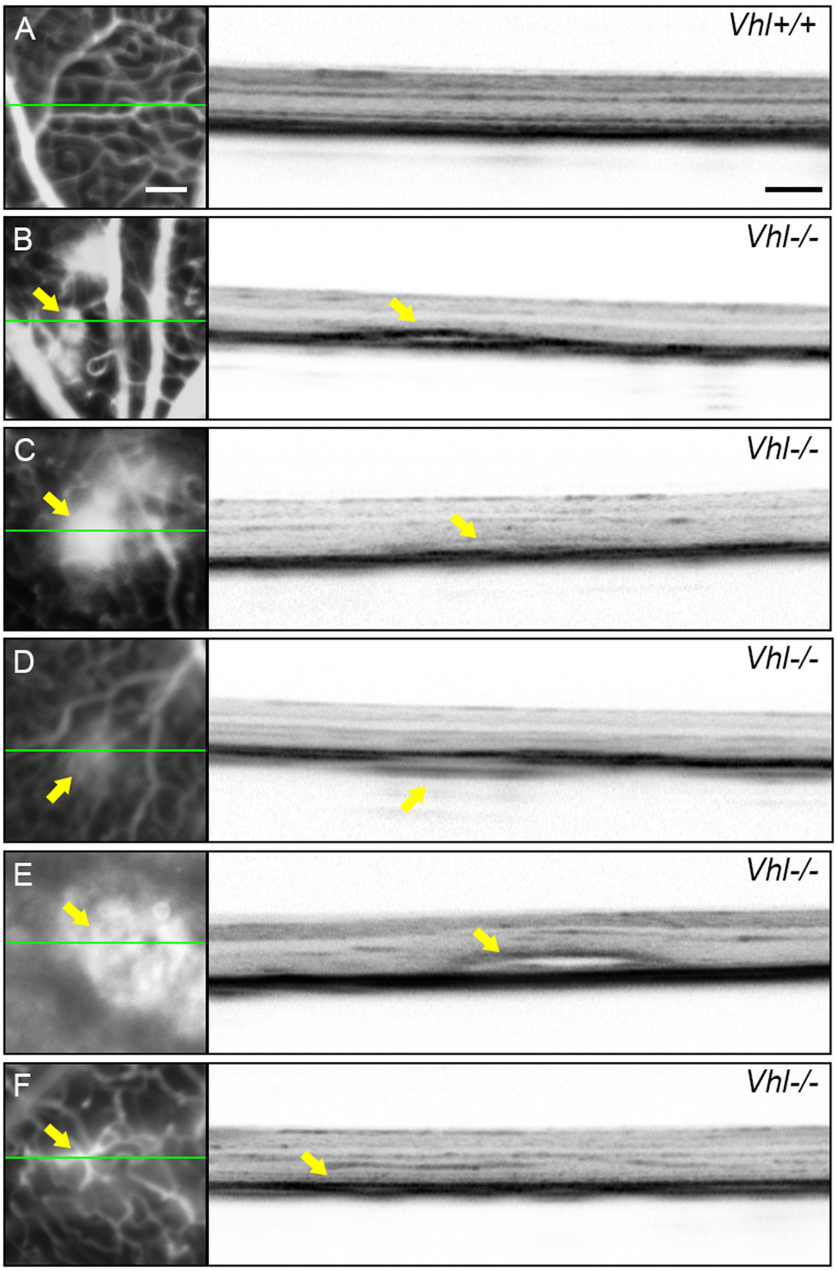

Figure 4. RPE detachments after $Vhl^{-/-}$ in photoreceptors in $Pde6g^{creERT2/+};Vhl^{-/-}$ mice. (**A**) An OCT cross section from the normal $Pde6g^{creERT2/+};Vhl^{flox/flox}$ mouse model shows normal retinal layers. (**B–F**) OCT images from the tamoxifen-treated $Pde6g^{creERT2/+};Vhl^{-/-}$ mouse model. OCT sections were imaged over leakage sites (indicated by the green line in the accompanying FFA images). RPE detachment (**B**), lifted inner and outer segment layers and RPE tear (**C**), a break in the Bruch's membrane and an abnormal structure in the choroid layer (**D**), subretinal fluid (**E**) and hyperreflectivity in the outer retina (**F**) were observed in the mutant mouse model (green line = OCT scan; yellow arrows = abnormal lesions and structural findings in FFA and OCT images, respectively; white scale bar = 200 μm for all FFA images; black scale bar = 200 μm for all OCT images).

To our knowledge, our studies on the $Pde6g^{creERT2/+};Vhl^{-/-}$ mouse have been the first to provide direct evidence that photoreceptor hypoxia is necessary and sufficient for the development and progression of type 3 neovascularization. Our study also elucidated the specific locations in which neovascularization can occur in the retina as a result of induced hypoxia in rod photoreceptors. Moreover, given that Type 3 neovascularization does not occur in children, a significant translational value of the $Pde6g^{creERT2/+};Vhl^{-/-}$ preclinical model is its precision in mimicking exudative AMD progression in adult animals. Preclinical models that precisely phenocopy human pathophysiology would propel the development of novel therapies (26).

Materials and Methods

Mice

Mice were used in accordance with the *Statement for the Use of Animals in Ophthalmic and Vision Research* of the Association for Research in Vision and Ophthalmology (www.arvo.org/

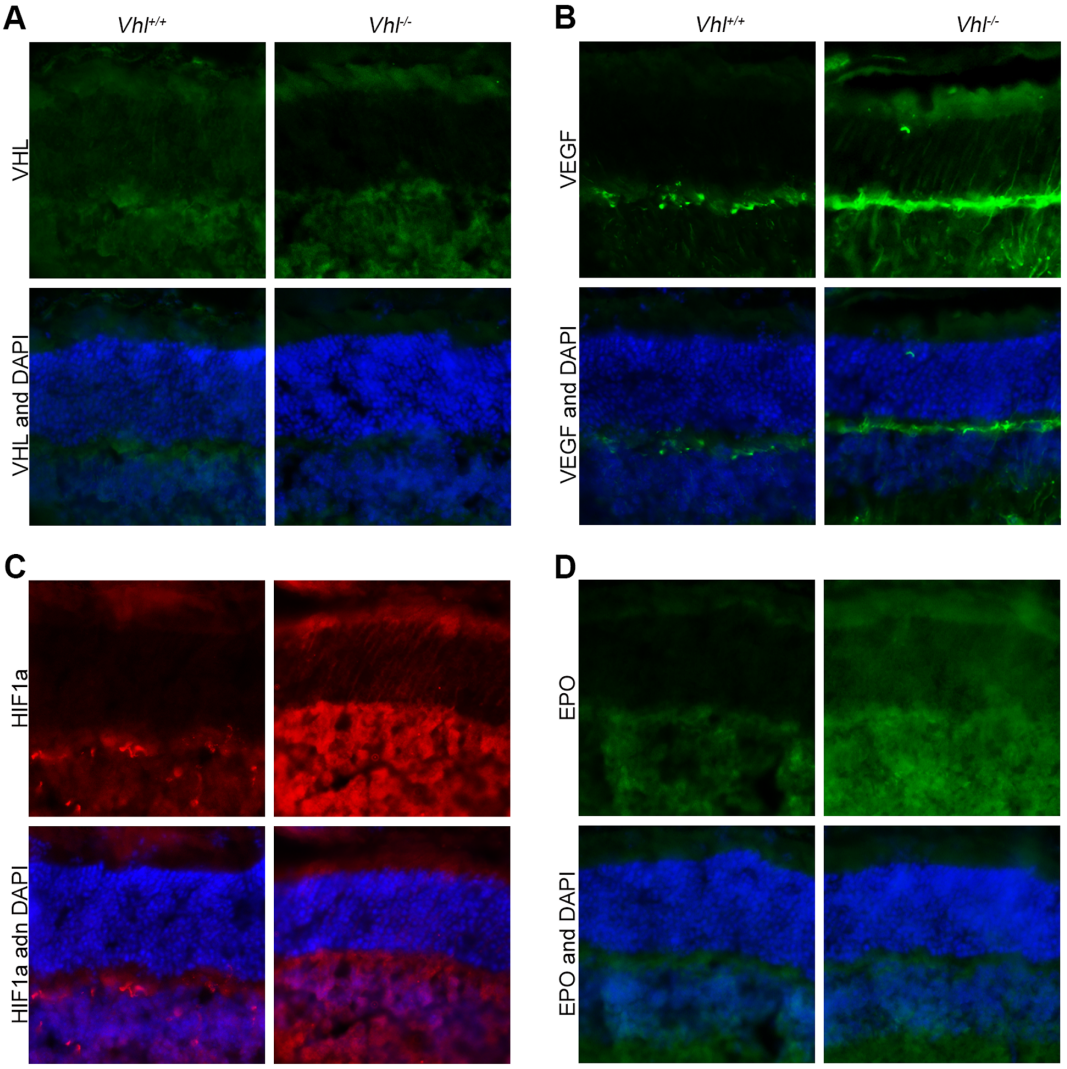

Figure 5. VEGF, HIF1a and EPO levels are increased after $Vhl^{-/-}$ in photoreceptors. Tamoxifen was administered to the $Pde6g^{creERT2/+};Vhl^{flox/flox}$ mouse model at P7 for 3 days. (**A**) Immunoreactivity of VHL and DAPI in both the $Pde6g^{creERT2/+};Vhl^{flox/flox}$ and $Pde6g^{creERT2/+};Vhl^{-/-}$ mouse retina. Immunofluorescence staining of VEGF (**B**), HIF1a (**C**) and EPO (**D**) in both the $Pde6g^{creERT2/+};Vhl^{flox/flox}$ and $Pde6g^{creERT2/+};Vhl^{-/-}$ mouse retina (white scale bar = 50 µm; blue = DAPI; green in A = anti-VHL; green in B = anti-VEGF; red = anti-HIF1a; green in D = anti-EPO).

About_ARVO/Policies/Statement_for_the_Use_of_Animals_in_Ophthalmic_and_Visual_Research/) and the *Policy on the Use of Animals in Neuroscience Research* of the Society for Neuroscience (https://www.sfn.org/advocacy/policy-positions/policies-on-the-use-of-animals-and-humans-in-research). All mice were housed in the Columbia University Pathogen-free Eye Institute Annex Animal Care Services Facility and maintained under a 12 h light–dark cycle. $Vhl^{flox/flox}$ mice [*C;129S-Vhl*^{tm1Jae}*/J*] were obtained from Jackson Laboratory (stock no. 004081). *Pde6g::Cre*^{ERT2} mice were generated at Jonas Children's Vision Care (27).

Multimodal live fundus imaging

Angiography, IR fundus and OCT images were obtained with the Spectralis OCT scanning laser confocal ophthalmoscope (OCT-SLO Spectralis 2; Heidelberg Engineering, Heidelberg, Germany) as previously described (28–30). In brief, pupils were dilated using topical 2.5% phenylephrine hydrochloride and 1% tropicamide (Akorn Inc., Lakeforest, IL, USA). When performing iris angiography, no dilation drops were applied to the mice. Mice were anesthetized by intraperitoneal injection of ketamine/xylazine when needed as described previously (31). During the procedure, body temperature was maintained at 37°C using a heating pad. Gonioscopic Prism solution (Akorn Inc., Lakeforest, IL, USA) was applied to both eyes to prevent dry eyes. The tested eye was washed with balanced salt water (Alcon Laboratories, Fort Worth, TX, USA). For FFA, a measure of 0.1 ml/10 g body weight (BW) of 10% AK-Fluor (25 mg/ml, Akorn Inc., Lakeforest, IL, USA) was injected intraperitoneally. Imaging was obtained at 488 nm absorption and 520 nm barrier filter using a 55° lens. IR fundus and angiography images of the central retina and peripheral retina were taken, with the optic nerve oriented at the center of the image or middle of the left-most part of the image, respectively. OCT images were acquired using a 30° lens with the automated real-time mode, using near-IR reflectance (820 nm) modalities. Images were analyzed by ImageJ (https://imagej.nih.gov/ij/; provided in the public domain by the NIH, Bethesda, MD, USA).

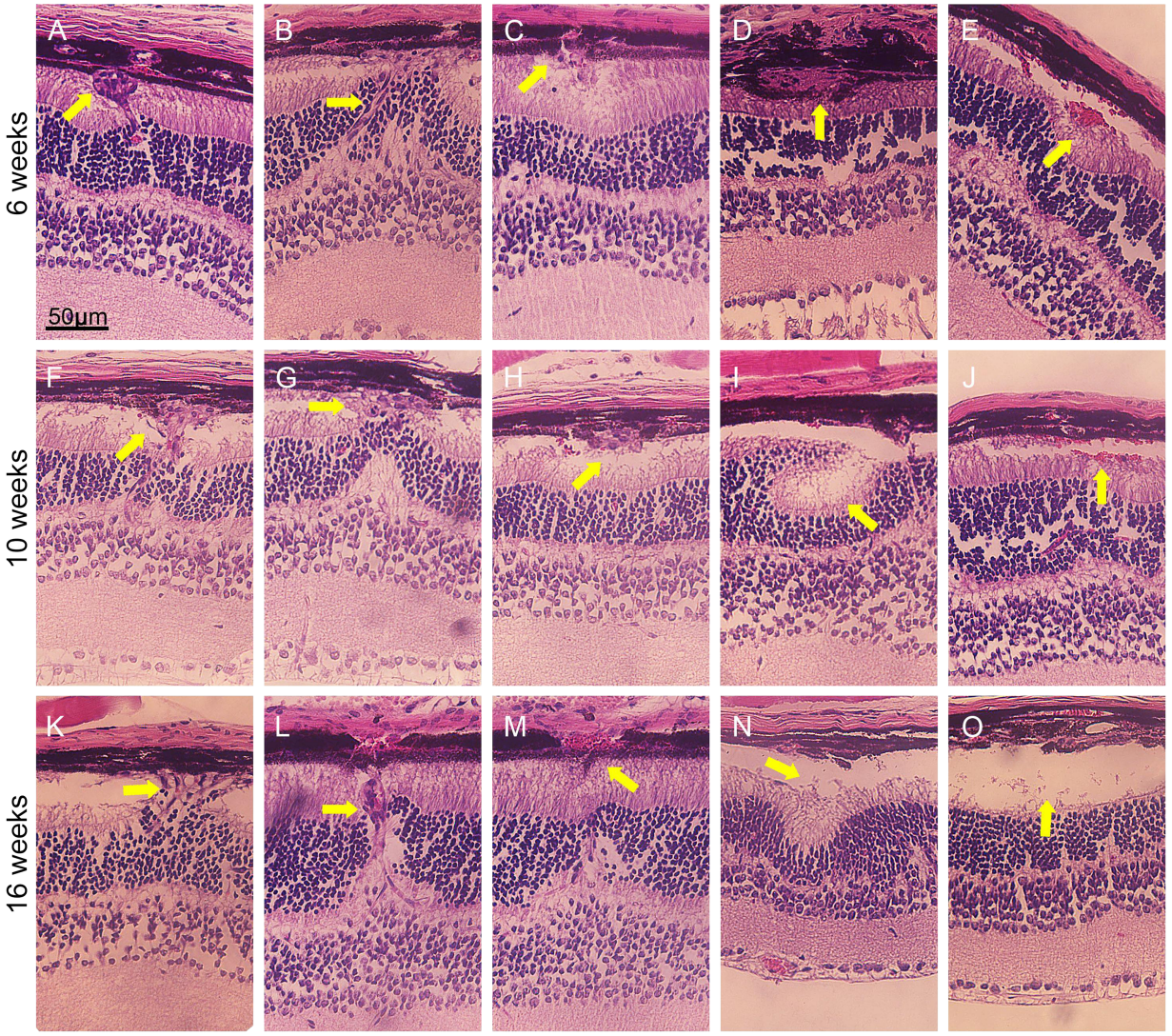

Figure 6. Subretinal neovascularization, hemorrhage, exudation, retinal folds and exudative detachment after $Vhl^{-/-}$. Tamoxifen was administered to $Pde6g^{creERT2/+};Vhl^{flox/flox}$ mice at P7 for 3 days to generate $Pde6g^{creERT2/+};Vhl^{-/-}$ mice. Eye cups were then harvested, and HE staining was performed to observe retinal structures at weeks 6 (**A–E**), 10 (**F–J**) and 16 (**K–O**) (yellow arrows = various retinal lesions; scale bar = 50 µm).

Tamoxifen administration

Tamoxifen (100 mg/ml in ethanol; Sigma-Aldrich T5648, St. Louis, MO, USA) was thoroughly mixed at 42°C and dilated with corn oil to a final concentration of 10 mg/ml. The solution was then injected intraperitoneally at a concentration of 100 µg/g BW for three consecutive days from postnatal day 7 (P7) or P28 (30).

Immunohistochemistry

Mice were euthanized following established Institutional Animal Care and Use Committee guidelines. Eyes were processed and sectioned as we described in our previous paper (30). Sections were incubated overnight at 4°C with primary antibodies: anti-CD31 (Abcam, ab28364, UK), anti-VHL (Thermo Fisher, MA5-13940, Waltham, MA, USA), anti-HIF1α (Abcam, ab16066, UK), anti-VEGF (Abcam, ab52917, UK) and anti-EPO (Santa Cruz, sc80995, Dallas, TX, USA). After washing with Phosphate Buffered Saline (PBS) with 0.3% Triton X-100 (PBST) three times for 10 min each, sections were incubated with the secondary antibody for 90 mins at room temperature. The following secondary antibodies were used: Alexa 555 or Alexa 488 (1:500, Molecular Probes, Life Technologies, Waltham, MA, USA). After incubating in 5 µg/ml Hoechst 33342 (H13999, Molecular Probes, Life Technologies, Waltham, MA, USA) for 5 min, sections were imaged using a confocal microscope (Nikon A1, Japan).

Whole-retina flat mount and iris flat mount immunohistochemistry

Retinae and irises were fixed in 4% paraformaldehyde for 20 min, washed and stained as described above. The images were then taken using a confocal microscope (Nikon A1, Japan).

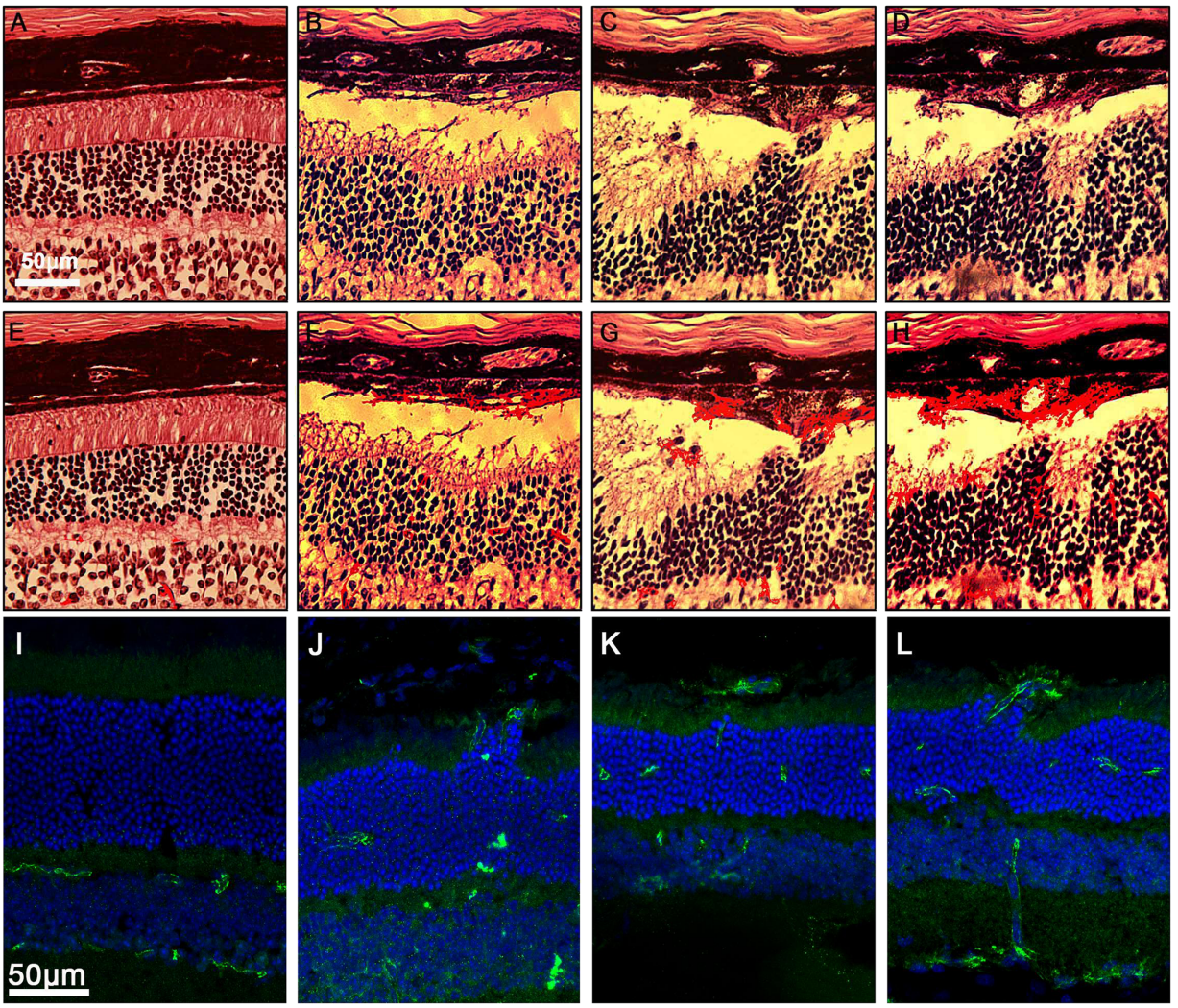

Figure 7. PAS and immunofluorescence staining of vessels in the retina revealed the location of neovascularization in *Pde6g*$^{creERT2/+}$;*Vhl*$^{-/-}$ mice compared to *Pde6g*$^{creERT2/+}$;*Vhl*$^{flox/flox}$ control. Tamoxifen was administered to *Pde6g*$^{creERT2/+}$;*Vhl*$^{flox/flox}$ mice at P7 for 3 days to induce *Vhl* knockout in rod photoreceptors. Optic cups were harvested at 10 weeks. (**A**) PAS staining of a retinal paraffin section from the *Pde6g*^{creERT2};*Vhl*$^{flox/flox}$ mouse at week 10. (**B–D**) PAS staining of retinal paraffin sections from the *Pde6g*^{creERT2};*Vhl* $^{-/-}$ mouse at week 10. (**E–H**) Duplicate images from A–D with vessel signals enhanced using ImageJ software. (**I**) Immunostaining of a retinal frozen section from the *Pde6g*^{creERT2};*Vhl* $^{flox/flox}$ mouse at week 10. (**J–L**) Immunostaining of retinal frozen sections from the *Pde6g*^{creERT2};*Vhl* $^{-/-}$ mouse at week 10 (white scale bars = 50 μm; blue = DAPI, green = anti-CD31).

Hematoxylin–eosin staining

Mice were euthanized and eyes were enucleated and fixed. Hematoxylin–eosin (HE) histologic analysis was carried out as described previously (32).

PAS staining

Optic cups were collected as described above, fixated in 10% formalin, embedded in Paraffin and then sectioned at 5 μm. After 5 min of oxidation in 0.5% periodic acid solution (NovaUltra TM, PAS stain kit, #IW-3009), the optic cup sections were rinsed and placed in Schiff reagent for 15 min. Sections were then washed in lukewarm tap water for 5 min, counterstained in Mayer's hematoxylin for 1 min and washed again for 5 min before getting dehydrated and mounted on a coverslip using a synthetic mounting medium.

Histologic analysis

Mice were euthanized, and eyes were processed and sectioned. HE or PAS histologic analysis was carried out as described previously (33).

Statistical analysis

Statistical analysis was performed using GraphPad Prism, version 6 (GraphPad Software, CA, USA); $^{*}P < 0.05$ was treated as statistically significant, with greater statistical significance denoted as $^{**}P < 0.01$ and $^{***}P < 0.001$.

Author contributions

S.H.T. and L.Z. designed the experiments; L.Z., X.C. and YJ.H. conducted the experiments; S.H.T., X.C. and K.S.P. composed the

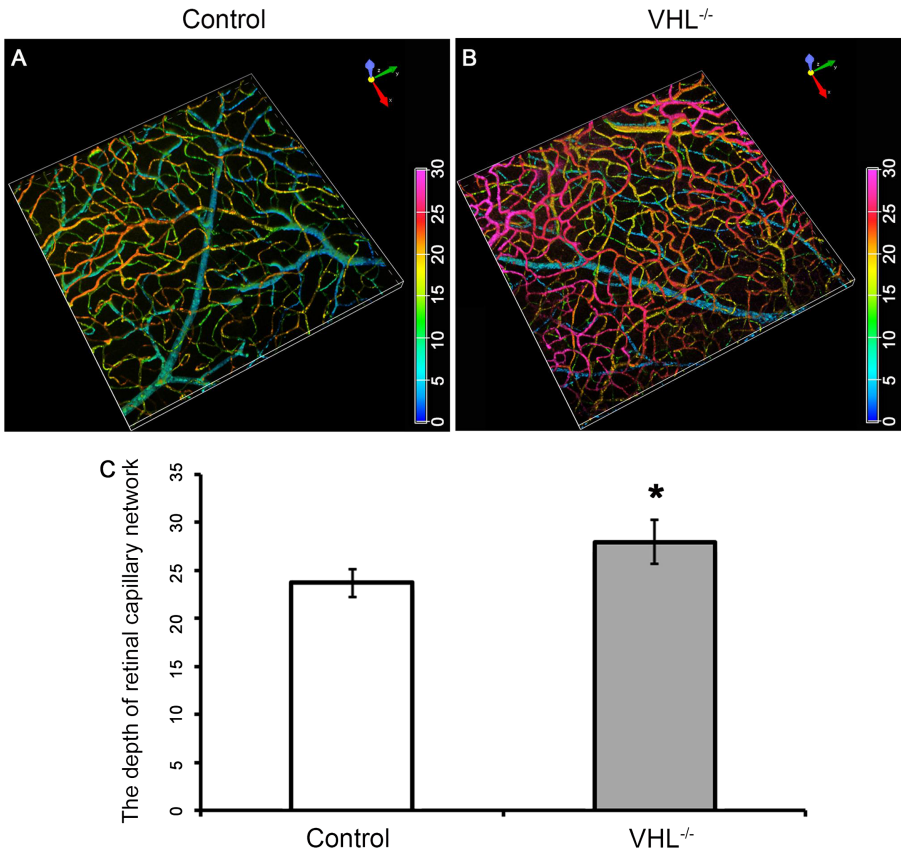

Figure 8. Increased capillary density after $Vhl^{-/-}$ in the $Pde6g^{creERT2/+};Vhl^{-/-}$ mouse model. 3D remodeling of the vessels with immunofluorescence staining in the retinal flat mount in a $Pde6g^{creERT2/+};Vhl^{flox/flox}$ (**A**) and $Pde6g^{creERT2/+};Vhl^{-/-}$ (**B**) mouse at week 6. (**C**) Bar graphs quantifying the depth of retinal capillary network measured in the retinal flat mounts from control and $Vhl^{-/-}$ mice. Anti-CD31 was used as primary antibody (color spectrum = depth of blood vessels within the retina; $^{*}P < 0.05$).

manuscript; L.Z. collected the data; X.C. and Y.J.H. analyzed the data; L.Z., X.C. and YJ.H. prepared the images and figures; X.G., X.Z., Z.Y., Y.H., C.-W. H., A.B. and V.M. provided technical support; S.H.T. and L.Z. obtained funding; S.H.T supervised the study and provided all materials and administrative support.

Supplementary Material

Supplementary Material is available at HMG online.

Conflicts of Interest statement

None declared.

Funding

National Natural Science Foundation of China (81500750 to L.Z.); Shanxi Health and Family Planning Commission (2018088 to L.Z.); The Jonas Children's Vision Care and Bernard & Shirlee Brown Glaucoma Laboratory are supported by the National Institutes of Health (P30EY019007, R01EY018213 and R01EY024698), National Cancer Institute Core (5P30CA013696), NYSTEM IIRP Contract C32590GG, Edward N. & Della L. Thome Memorial Foundation, Foundation Fighting Blindness (TA-NMT-0116-0692-COLU), Kobi and Nancy Karp, the Crowley Family Fund, the Rosenbaum Family Foundation, the Tistou and Charlotte Kerstan Foundation, the Schneeweiss Stem Cell Fund, New York State (C029572) and the Gebroe Family Foundation, Research to Prevent Blindness (RPB) Physician–Scientist Award and unrestricted funds from RPB, New York, NY, USA. S.H.T. is a member of the RD-CURE Consortium.

References

1. Country, M.W. (2017) Retinal metabolism: a comparative look at energetics in the retina. *Brain Res.*, **1672**, 50–57.
2. Sivaprasad, S. and Arden, G. (2016) Spare the rods and spoil the retina: revisited. *Eye (Lond.)*, **30**, 189–192.
3. Arden, G.B., Sidman, R.L., Arap, W. and Schlingemann, R.O. (2005) Spare the rod and spoil the eye. *Br. J. Ophthalmol.*, **89**, 764–769.
4. Lin, M.K., Kim, S.H., Zhang, L., Tsai, Y.T. and Tsang, S.H. (2015) Rod metabolic demand drives progression in retinopathies. *Taiwan J. Ophthalmol.*, **5**, 105–108.
5. Bressler, N.M. (2004) Age-related macular degeneration is the leading cause of blindness. *JAMA*, **291**, 1900–1901.
6. Barben, M., Samardzija, M. and Grimm, C. (2018) The role of hypoxia, hypoxia-inducible factor (HIF), and VEGF in retinal angiomatous proliferation. *Adv. Exp. Med. Biol.*, **1074**, 177–183.
7. Klein, R., Klein, B.E., Tomany, S.C., Meuer, S.M. and Huang, G.H. (2002) Ten-year incidence and progression of age-related maculopathy: the beaver dam eye study. *Ophthalmology*, **109**, 1767–1779.
8. Lynn, S.A., Keeling, E., Munday, R., Gabha, G., Griffiths, H., Lotery, A.J. and Ratnayaka, J.A. (2017) The complexities

underlying age-related macular degeneration: could amyloid beta play an important role? *Neural Regen. Res.*, **12**, 538–548.
9. Chappelow, A.V. and Kaiser, P.K. (2008) Neovascular age-related macular degeneration: potential therapies. *Drugs*, **68**, 1029–1036.
10. Stewart, M.W. (2012) The expanding role of vascular endothelial growth factor inhibitors in ophthalmology. *Mayo Clin. Proc.*, **87**, 77–88.
11. Waisbourd, M., Loewenstein, A., Goldstein, M. and Leibovitch, I. (2007) Targeting vascular endothelial growth factor: a promising strategy for treating age-related macular degeneration. *Drugs Aging*, **24**, 643–662.
12. Zylbermann, R., Landau, D., Rozenman, Y., Abrahami, S. and Pollack, A. (1997) Exudative age-related macular degeneration in patients with diabetic retinopathy and its relation to retinal laser photocoagulation. *Eye (Lond.)*, **11**(Pt 6), 872–875.
13. Feigl, B. (2009) Age-related maculopathy - linking aetiology and pathophysiological changes to the ischaemia hypothesis. *Prog. Retin. Eye Res.*, **28**, 63–86.
14. Lin, C., McGough, R., Aswad, B., Block, J.A. and Terek, R. (2004) Hypoxia induces HIF-1alpha and VEGF expression in chondrosarcoma cells and chondrocytes. *J. Orthop. Res.*, **22**, 1175–1181.
15. Schmidt-Erfurth, U., Chong, V., Loewenstein, A., Larsen, M., Souied, E., Schlingemann, R., Eldem, B., Mones, J., Richard, G., Bandello, F. *et al.* (2014) Guidelines for the management of neovascular age-related macular degeneration by the European Society of Retina Specialists (EURETINA). *Br. J. Ophthalmol.*, **98**, 1144–1167.
16. Miller, J.W., Le Couter, J., Strauss, E.C. and Ferrara, N. (2013) Vascular endothelial growth factor a in intraocular vascular disease. *Ophthalmology*, **120**, 106–114.
17. Maxwell, P.H., Wiesener, M.S., Chang, G.W., Clifford, S.C., Vaux, E.C., Cockman, M.E., Wykoff, C.C., Pugh, C.W., Maher, E.R. and Ratcliffe, P.J. (1999) The tumour suppressor protein VHL targets hypoxia-inducible factors for oxygen-dependent proteolysis. *Nature*, **399**, 271–275.
18. Datta, K., Mondal, S., Sinha, S., Li, J., Wang, E., Knebelmann, B., Karumanchi, S.A. and Mukhopadhyay, D. (2005) Role of elongin-binding domain of von Hippel Lindau gene product on HuR-mediated VPF/VEGF mRNA stability in renal cell carcinoma. *Oncogene*, **24**, 7850–7858.
19. Tobe, T., Okamoto, N., Vinores, M.A., Derevjanik, N.L., Vinores, S.A., Zack, D.J. and Campochiaro, P.A. (1998) Evolution of neovascularization in mice with overexpression of vascular endothelial growth factor in photoreceptors. *Invest. Ophthalmol. Vis. Sci.*, **39**, 180–188.
20. Chen, Y., Hu, Y., Lu, K., Flannery, J.G. and Ma, J.X. (2007) Very low density lipoprotein receptor, a negative regulator of the wnt signaling pathway and choroidal neovascularization. *J. Biol. Chem.*, **282**, 34420–34428.
21. Tiebel, O., Oka, K., Robinson, K., Sullivan, M., Martinez, J., Nakamuta, M., Ishimura-Oka, K. and Chan, L. (1999) Mouse very low-density lipoprotein receptor (VLDLR): gene structure, tissue-specific expression and dietary and developmental regulation. *Atherosclerosis*, **145**, 239–251.
22. Qiu, G., Stewart, J.M., Sadda, S., Freda, R., Lee, S., Guven, D., de Juan, E.J. and Varner, S.E. (2006) A new model of experimental subretinal neovascularization in the rabbit. *Exp. Eye Res.*, **83**, 141–152.
23. Baffi, J., Byrnes, G., Chan, C.C. and Csaky, K.G. (2000) Choroidal neovascularization in the rat induced by adenovirus mediated expression of vascular endothelial growth factor. *Invest. Ophthalmol. Vis. Sci.*, **41**, 3582–3589.
24. Spilsbury, K., Garrett, K.L., Shen, W.Y., Constable, I.J. and Rakoczy, P.E. (2000) Overexpression of vascular endothelial growth factor (VEGF) in the retinal pigment epithelium leads to the development of choroidal neovascularization. *Am. J. Pathol.*, **157**, 135–144.
25. Wang, F., Rendahl, K.G., Manning, W.C., Quiroz, D., Coyne, M. and Miller, S.S. (2003) AAV-mediated expression of vascular endothelial growth factor induces choroidal neovascularization in rat. *Invest. Ophthalmol. Vis. Sci.*, **44**, 781–790.
26. Pennesi, M.E., Neuringer, M. and Courtney, R.J. (2012) Animal models of age related macular degeneration. *Mol. Aspects Med.*, **33**, 487–509.
27. Koch, S.F., Tsai, Y.T., Duong, J.K., Wu, W.H., Hsu, C.W., Wu, W.P., Bonet-Ponce, L., Lin, C.S. and Tsang, S.H. (2015) Halting progressive neurodegeneration in advanced retinitis pigmentosa. *J. Clin. Invest.*, **125**, 3704–3713.
28. Seeliger, M.W., Beck, S.C., Pereyra-Munoz, N., Dangel, S., Tsai, J.Y., Luhmann, U.F., van de Pavert, S.A., Wijnholds, J., Samardzija, M., Wenzel, A. *et al.* (2005) In vivo confocal imaging of the retina in animal models using scanning laser ophthalmoscopy. *Vision Res.*, **45**, 3512–3519.
29. Wert, K.J., Mahajan, V.B., Zhang, L., Yan, Y., Li, Y., Tosi, J., Hsu, C.W., Nagasaki, T., Janisch, K.M., Grant, M.B. *et al.* (2016) Neuroretinal hypoxic signaling in a new preclinical murine model for proliferative diabetic retinopathy. *Signal Transduct. Target. Ther.*, **1**.
30. Zhang, L., Cui, X., Jauregui, R., Park, K.S., Justus, S., Tsai, Y.T., Duong, J.K., Hsu, C.W., Wu, W.H., Xu, C.L. *et al.* (2018) Genetic rescue reverses microglial activation in preclinical models of retinitis pigmentosa. *Mol. Ther.*, **26**, 1953–1964.
31. Zhang, L., Du, J., Justus, S., Hsu, C.W., Bonet-Ponce, L., Wu, W.H., Tsai, Y.T., Wu, W.P., Jia, Y., Duong, J.K. *et al.* (2016) Reprogramming metabolism by targeting sirtuin 6 attenuates retinal degeneration. *J. Clin. Invest.*, **126**, 4659–4673.
32. Sancho-Pelluz, J., Tosi, J., Hsu, C.W., Lee, F., Wolpert, K., Tabacaru, M.R., Greenberg, J.P., Tsang, S.H. and Lin, C.S. (2012) Mice with a D190N mutation in the gene encoding rhodopsin: a model for human autosomal-dominant retinitis pigmentosa. *Mol. Med.*, **18**, 549–555.
33. Tsai, Y.T., Wu, W.H., Lee, T.T., Wu, W.P., Xu, C.L., Park, K.S., Cui, X., Justus, S., Lin, C.S., Jauregui, R. *et al.* (2018) Clustered regularly interspaced short palindromic repeats-based genome surgery for the treatment of autosomal dominant retinitis pigmentosa. *Ophthalmology*, **125**, 1421–1430.